

GEOTHERMOBAROMETRY OF AMPHIBOLES IN GRANITOID ROCKS FROM THE BAGHCHE MARYAM AREA, SANANDAJ-SIRJAN ZONE, NW IRAN**GEOTERMOBAROMETRIA DE ANFÍBOLAS EM ROCHAS GRANITÓIDES DA ÁREA BAGHCHE MARYAM, NA ZONA SANANDAJ-SIRJAN, NOROESTE DO IRÃ**

Farhad Sheikhi¹

Seyed Mohamad Hosein Razavi²

Zohreh Alaminia³

Mohamad Lotfi⁴

ABSTRACT

The Baghche Maryam (BM) granitoid body is located in the northern part of the Sanandaj-Sirjan zone (SSZ), NW Iran. The BM intrusion is composed of diorite, monzodiorite, syenite and granite with a calc-alkaline to alkaline affinity. Mafic minerals in the BM rocks are biotite and Amphibole. Amphiboles are calcic (magnesiohornblende). The emplacement pressure average of the BM intrusion for granite and diorite rocks is 2.14 and 2.33+0.6 kbar, respectively. During the evolution of this magmatic system to higher silica contents, there was an increase in the activity of oxygen and a decrease in the temperature and the emplacement depth from the monzogabbro-monzodiorite to granite rocks; this is consistent with the typical evolution of the granitoid rocks. The studied amphibole rims show the calculated higher temperature and pressure and low fO₂ and H₂O content than the core of amphiboles which reflects differences in emplacement depth and crystallization conditions.

Keywords: Granitoid Rocks; Geothermobarometry; Baghche Maryam; Sanandaj-Sirjan Zone; Iran.

RESUMO

A área granítóide baghche maryam (bm) está localizado na parte norte da zona de sanandaj-sirjan (ssz), nw irã. a intrusão bm é composta por diorito, monzodiorito, sienito e granito com afinidade cálcico-alcalina a alcalina. os minerais máficos nas rochas bm são biotita e anfibólio.

¹Department of Geology, North Tehran Branch, Islamic Azad University, Tehran, Iran. sheikh.farhad@gmail.com
ORCID: <https://orcid.org/0000-0003-1124-7087>

²Department of Geology, North Tehran Branch, Islamic Azad University, Tehran, Iran. razavi.khu@gmail.com
ORCID: <https://orcid.org/0000-0002-8223-8332>

³Department of Geochemistry, Faculty of Earth Sciences, Kharazmi University, Tehran, Iran
zoalaminia@gmail.com ORCID: <https://orcid.org/0000-0002-6576-1615>

⁴Department of Geology, North Tehran Branch, Islamic Azad University, Tehran, Iran. m_ltifi_1014@yahoo.com
ORCID: <https://orcid.org/0000-0002-5414-1381>

os anfibólios são cárquicos (magnesiohornblende). a pressão de colocação média da intrusão bm para rochas de granito e diorito é 2,14 e 2,33 + 0,6 kbar, respectivamente. durante a evolução desse sistema magmático para maiores teores de sílica, houve um aumento na atividade do oxigênio e uma diminuição na temperatura e na profundidade de colocação do monzogabbro-monzdiorito para rochas graníticas; isso é consistente com a evolução típica das rochas granítoides. os anéis de anfibólio estudados mostram a temperatura e pressão mais altas calculadas e o baixo teor de fo2 e h2o do que o núcleo dos anfibólios, o que reflete as diferenças na profundidade de colocação e nas condições de cristalização.

Palavras-chave: Rochas granítoides; Geotermobarometria; Baghche maryam; Zona Sanandaj-sirjan; Irã.

INTRODUCTION

Amphiboles occur as rock-forming minerals in a wide variety of composition and structure. The International Mineralogical Association (IMA) classifies amphiboles as a mineral supergroup, within which are two groups and several subgroups (LEAKE *et al.*, 1997, 2004). This classification is important for geothermobarometric studies. Some amphiboles, such as actinolite, are created through subsolidus and secondary processes (LEAKE, 1971; HELMY *et al.*, 2004) and thus are not used in geothermobarometric studies. Amphiboles, especially hornblende, are the most widely used minerals for geothermobarometry because they occur in calc-alkaline intrusive bodies with various compositions. They are stable over a wide P-T range of 1–23 kbar and 400–1150 °C. Al content in amphibole and amphibole composition varies depending on the bulk composition of magma, temperature, oxygen fugacity, and pressure during crystallization. Increasing temperature and pressure increase Al content in amphiboles, and their effects are considerably greater than those of the two other factors (MOODY *et al.*, 1983). In the last three decades, Al geobarometry in amphiboles has been widely used to calculate the crystallization pressure of magma and to determine the emplacement depth of batholiths in the earth's crust (HAMMARSTROM, ZEN, 1986; HOLLISTER *et al.*, 1987; JOHNSON, RUTHERFORD, 1989; RUTTER *et al.*, 1989; VYHNAL *et al.*, 1991; SCHMIDT, 1992; LEAKE , SAID, 1994; AGUE, BRANDON, 1996; ANDERSON, 1996; STEIN, DIETL, 2001; ERNST, 2002; MOAZZEN, DROOP, 2005; ZHANG *et al.*, 2006; UCHIDA *et al.*, 2007;

ANDERSON *et al.*, 2008; HOSSAIN *et al.*, 2009). Knowledge of solidification depth of calc-alkaline plutons is critical to understanding and unraveling the complex spatial, temporal, and chemical evolution of orogenic belts (RUTTER *et al.*, 1989).

In the northern Sanandaj-Sirjan Zone (SSZ), northwest Iran, a variety of granitoid bodies emplaced in several stages during Mesozoic times (MOHAJJEL *et al.*, 2003). The Baghche Maryam (BM) intrusion is a major granitoid in the northern part of the SSZ (Figure 1a), that emplaced at ca. 145.7+1.1 Ma (AZIZI *et al.*, 2016). The limited availability of published research on the BM intrusion underscores that little is currently understood about this type of rock. The present study aims to estimate the crystallization temperature and pressure of amphiboles in granitoid rocks from the BM area. It also is used to quantitatively reconstruct the emplacement depth of the pluton and interpretation of the Sanandaj–Sirjan magmatic–metamorphic belt, Iran.

GEOLOGICAL SETTING

The Sanandaj–Sirjan zone (SSZ) is a narrow NW–SE trending orogenic belt located in the western part of the Iranian Plate (Figure 1a). The SSZ is known as a polyphase terrain, experiencing several episodes of deformation, metamorphism and magmatism through time (HASSANZADEH *et al.*, 2008; MOHAJJEL *et al.*, 2003; TILLMAN *et al.*, 1981).

The basement of the SSZ mainly consists of a Precambrian complex, which has been exhumed from beneath Triassic-Jurassic metamorphic rocks and occurs as a tectonic window. The Triassic-Jurassic metamorphic rocks are overlain by the Cretaceous non-metamorphic rocks, especially in the southern parts (MOHAJJEL, FERGUSSON, 2014; MOHAJJEL *et al.*, 2003) and in the northwest of Iran between the cities of Ghorveh and Sanandaj. From north to south, the SSZ can be divided into two main parts (Figure 1a): the northern part contains various granitoid bodies that were intruded into the Triassic-Jurassic metamorphic complex, and they have ages of 180–140 Ma (MAHMOUDI *et al.*, 2011; AZIZI *et al.*, 2011a, 2011b; AZIZI, ASAHIARA 2013; AZIZI *et al.*, 2015a, 2015b; SHAHBAZI *et al.*, 2015; YAJAM *et al.*, 2015; AZIZI

et al., 2016). The abundance and distribution of granitoids in the northern SSZ, especially in the area from Azna to Ghorveh, are much greater and wider than in other parts of the SSZ (MOHAJJEL, FERGUSSON, 2014). The BM area, which is part of the northern SSZ, includes a Triassic–Jurassic metamorphic complex with marble, amphibolite, green schist, meta-chert and quartzite, which were deformed and show poly-deformation structures (Figure 2a). The metamorphic rocks are cut by the Middle to Late Jurassic granitoid body (AZIZI *et al.*, 2016). The Late Jurassic BM intrusion has a sigmoid-shape, NW-SE extending trend, with smooth weathering surfaces. The BM intrusion is composed of a variety of petrographic types, including granite, syenite, monzodiorite, diorite and gabbrodiorite. It contains fine to medium-grained mafic microgranular enclaves with diorite to gabbrodiorite composition (Figure 2b). The intrusion is often cut by leucogranite aplite-pegmatite dikes (Figure 2c) and quartz veins, which have a radial relationship with the contacts (Figure 2d).

SAMPLING AND ANALYTICAL METHODS

A total of 120 samples was collected from the BM intrusive rocks to undertake petrographic and mineral chemistry studies. The petrographic studies include identification of mineral assemblages, textures, alteration and metasomatic replacements. Mineral abundance was calculated based on modal mineral content; i.e., the actual mineral content is given in volume%. The modal analysis was performed using an Olympus BX60 microscope. Based on optical microscopic observations, nine samples were selected for whole rock chemical analyses. Major element analyses of the fresh nine samples were performed using a PANalytical Axios Advanced X-ray fluorescence (XRF) on fused glass beads, composed of sample material and lithium borate flux of 1:5 ratio, in order to eliminate mineralogical effects and reduce inter-element effects. Trace and rare earth elements (REEs) were analyzed using an Agilent 7700 x inductively coupled plasma-mass spectrometry (ICP-MS), following lithium meta-borate fusion and HNO₃ total digestion. The analytical error for most elements is less than 2%. The detection limit for trace elements and REEs analysis is 0.01 to 0.1 ppm.

Eight polished-thin sections of amphibole mineral from the BM intrusive rocks were selected for electron probe microanalyser (EPMA). EPMA analyses were obtained using a Cameca SX-50. Mineral compositions were determined by wavelength dispersive X-ray spectrometry (WDX) analysis for all measured elements. The system's five WDS spectrometers were equipped with PET, LIF, PET, TAP and TAP crystals. Operating conditions were as follows: acceleration voltage of 15 kV, beam current of 15 nA, and beam diameter of 10 µm (to avoid light element migration) for amphibole. Acquisition times were selected as 20 s on peak and 10 s on each background. Elements were calibrated against synthetic and natural standards.

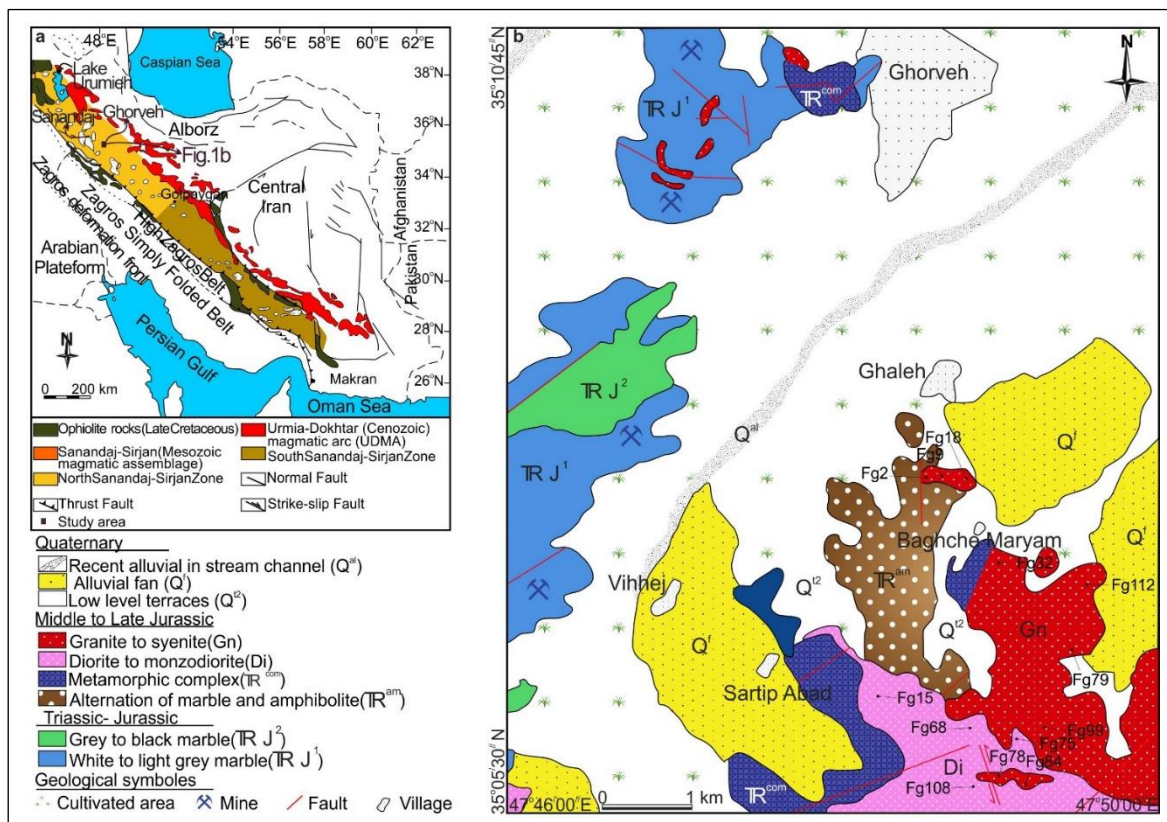


Figure 1. (a) Simplified tectonic map of Iran showing the Sanandaj–Sirjan zone (SSZ) Study area is within the quadrangle in the west of the map; (b) Detailed geologic map of the Baghche Maryam (BM) area showing distribution of Jurassic granitoid bodies in the study area. Sample names and locations are shown.

Source: Modified from DILEK *et al.* (2010); MOHAJJEL and FERGUSSON (2003).

PETROGRAPHY

On the basis of the results of thin section observations, the BM intrusive rocks were classified into two groups. The first group is labeled as gabbroic diorite, diorite and monzodiorite in the lithological map (Figure 1b). Outcrops of the gabbroic diorite rocks are rare, and the rocks are mainly observed as enclaves within the BM intrusion. The group is characterized by coarse to fine-grained textures, is green to black in color.

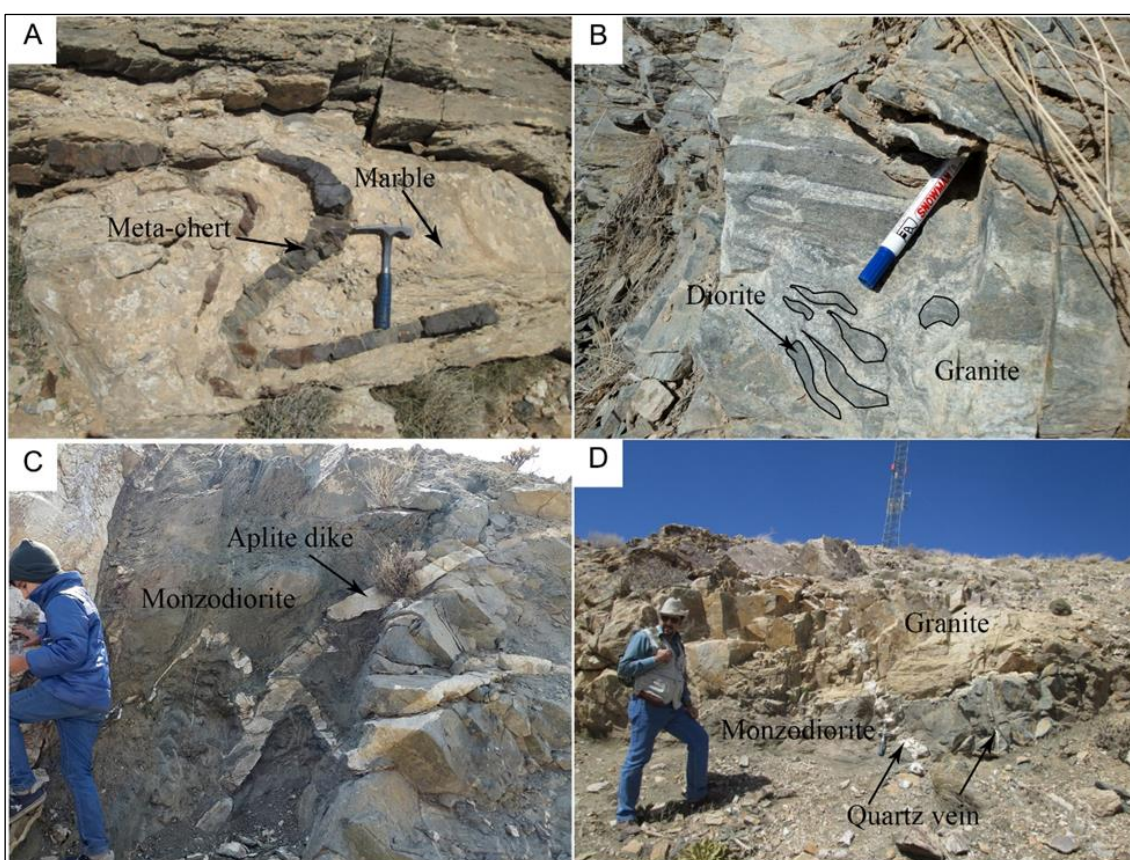


Figure 2. Exposures of intrusive and metamorphic rocks; (a) The host rocks are marble, meta-chert and amphibolite, which were deformed in the Late Jurassic (view to the northeast); (b) mafic microgranular enclaves of diorite within granite (view to the south); (c) leucogranite aplite dikes crosscut the monzodiorite rocks (view to the southwest); (d) Quartz veins indicate a final phase of injection in this area (view to the southwest).

Source: Authors (2020).

Diorite is coarse to fine-grained. The major minerals are Ca-plagioclase (45–60 vol%), amphibole (25–30 vol%), biotite (5–7 vol%) and pyroxene (<5 vol%). The minor minerals

include, K-feldspar, quartz, titanite, zircon, apatite, and opaque minerals. The secondary minerals include sericite, zoisite, clinzozoisite, chlorite, epidote and magnetite.

Monzodiorite is medium to fine-grained with magmatic texture and chilled margins. The major minerals include plagioclase (40-50 vol%), amphibole (20-25 vol%), orthoclase (10-15 vol%), quartz (5-10 vol%), biotite (2-5 vol%), and pyroxene (<5 vol%). The minor minerals are titanite, apatite, zircon and opaque minerals. The secondary minerals epidote, calcite, chlorite, sericite and actinolite.

The second group is labeled as granite and syenite in the lithological map (Gn in Fig. 1b). The group is characterized by medium to fine-grained textures, is white to dark gray in color.

Granite is the dominant rock in the BM area. Granite is medium to fine-grained. The major minerals include quartz (35-40 vol%), plagioclase (25-30 vol%), K-feldspar (15-25 vol%), biotite (10-15 vol%) and amphibole (5-8 vol%). The minor minerals include titanite, zircon, and apatite. The secondary minerals are sericite, epidote, and chlorite.

Syenite is medium to fine-grained. The major minerals include K-feldspar (25-30 vol%), plagioclase (10-15 vol%), quartz (5-15 vol%), amphibole (10-15 vol%), biotite (5-8 vol%), and pyroxene (<5 vol%). The minor minerals include titanite, apatite, zircon, and opaque minerals. The secondary minerals are kaolinite, sericite, chlorite, and actinolite.

GEOCHEMISTRY OF THE BM INTRUSION

Results of major and trace element analyses of representative samples of the BM intrusion are given in Table 1. In the (Na₂O+K₂O) vs. SiO₂ diagram (MIDDLEMOST, 1985), samples plot in granite, syenite and gabbrodiorite field (Figure 3a). In the MALI vs. SiO₂ diagram (FROST and FROST, 2008), data points lie in the calc-alkalic- to alkalic region (Fig 3b). In the A/NK vs. A/CNK diagram (MANIAR and PICCOLI, 1989) samples plot in the metaluminous I-Type to slightly peraluminous field (Figure 3c). In Ce and Na₂O+K₂O vs. 10000Ga/Al diagrams (WHALEN *et al.*, 1987), syenite and granite samples (acid rocks) plot

in the A-type granitoids field, whereas the BM intermediate to basic (gabbrodiorite) samples plot in the I- and S-type granitoids field (Figure 4a, Figure 4b). The results of a systematic geochemical study based on various diagrams show a positive correlation between SiO₂ and Rb, U and Th, and a negative correlation between SiO₂ and Al₂O₃, TiO₂, FeO, MgO, CaO, P₂O₅, Sr and Eu (Table 1). These trends reveal the differentiation of the plagioclase and some mafic minerals such as hornblende or clinopyroxene during magma crystallization. The BM intrusion contains low concentrations of trace elements such as V, Cr, Ni, Sr, Ba, Zr and ΣREEs. The BM samples show the enrichment of the LREEs, low abundance of HREE (e.g. Dy, Y, Yb, Lu). These properties are related to the subduction zone (Figure 5).

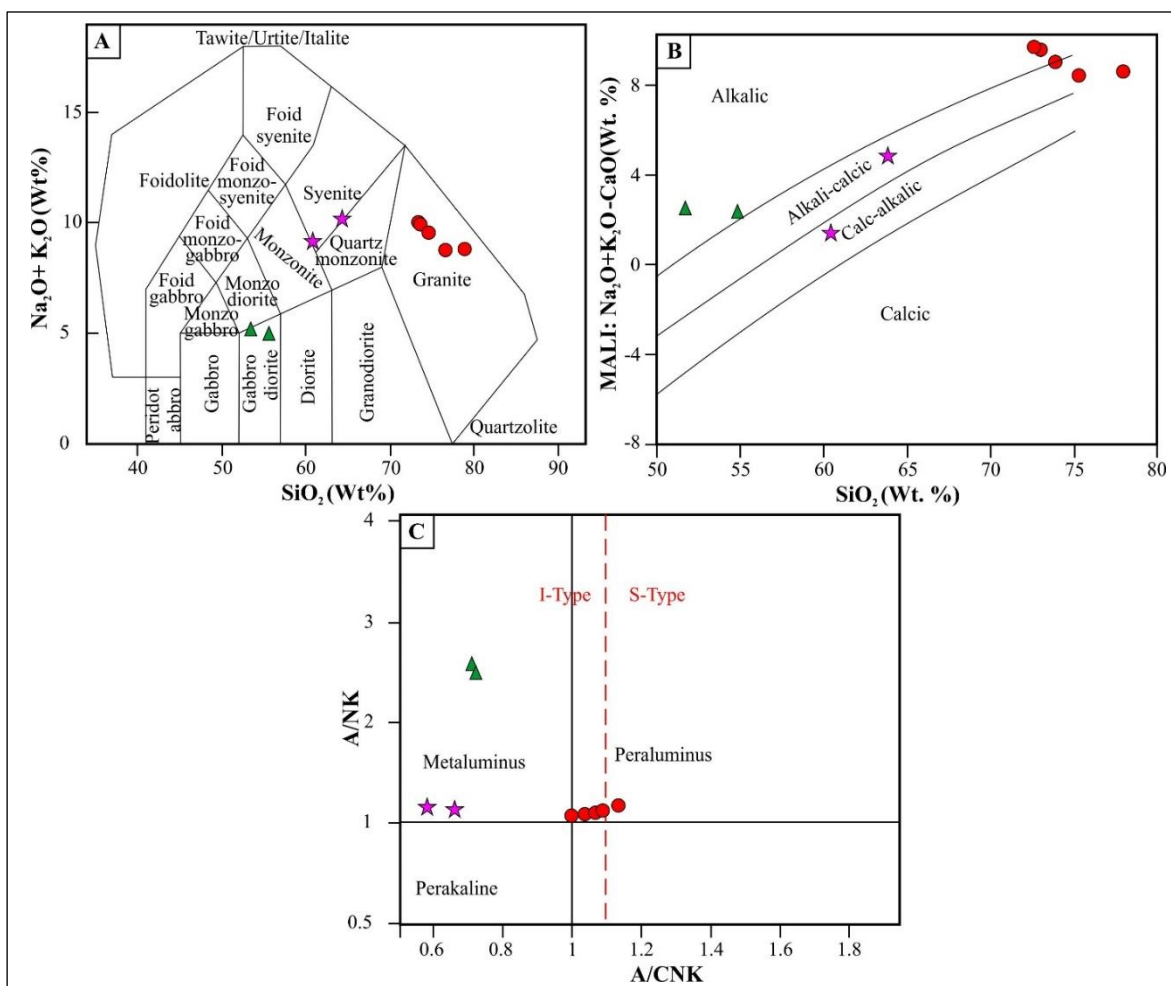


Figure 3. (a) Plot of the Baghche Maryam (BM) compositions in the SiO₂ vs. K₂O diagram; (b) Na₂O+K₂O-CaO vs. SiO₂ diagram; (c) A/NK vs. A/CNK diagram A=Al₂O₃, N=Na₂O, K=K₂O, and C=CaO (molar)

Source: MIDDLEMOST (1985); FROST and FROST (2008); MANIAR and PICCOLI, (1989)

*Symbols as in Figure 2.

CHEMISTRY OF AMPHIBOLES

Representative electron microprobe analyses of amphibole in the BM intrusion are given in Table 2.

Amphiboles are classified as “calcic amphibole” based on $(\text{Na}+\text{K})_{\text{A}} < 0.5$ and $\text{Ca}_{\text{A}} < 0.5$ (Leake *et al.* 1997). Calcic amphiboles are present in metaluminous to slightly peraluminous granitoid which belong to I-type magma (e.g. CHAPPELL and WHITE, 1974). $\text{Mg}/(\text{Mg}+\text{Fe}^{2+})$ ratio and Si content of amphiboles are 0.57-0.70 and 6.88-7.23 atom per formula unit (apfu) which are classified as magnesiohornblende (LEAKE *et al.*, 1997) (Fig. 6). Amphibole compositions with Si > 7.3 apfu are derived via the subsolidus process (AGEMAR *et al.*, 1997). None of the amphiboles from the BM intrusion were formed through the subsolidus process. Thus, all of them are suitable and selected for geothermobarometry.

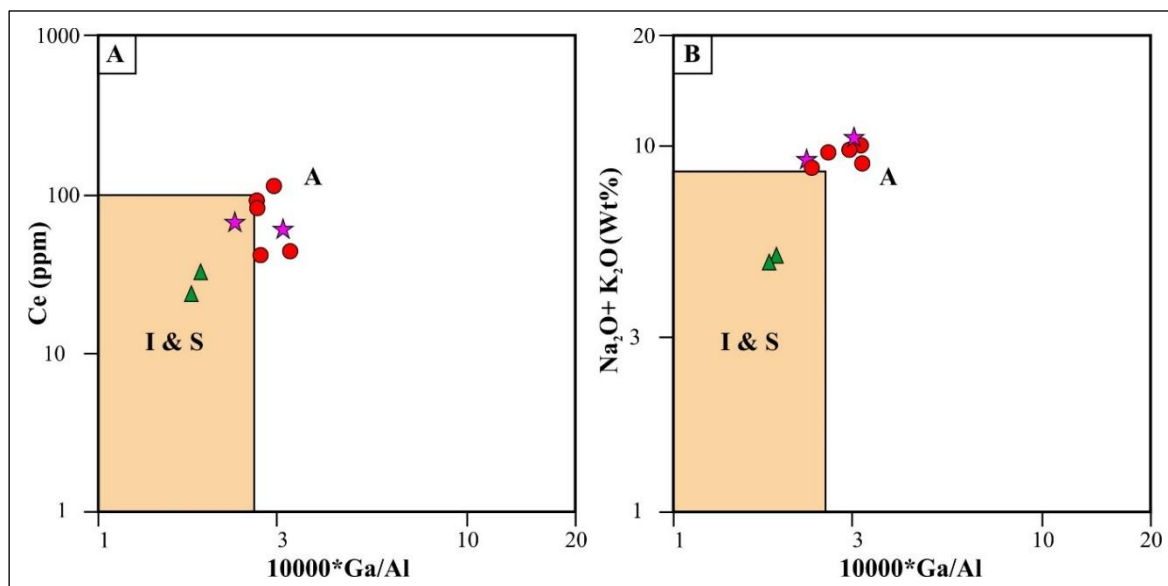


Figure 4. A-type granite discrimination diagram for the BM intrusion

Source: WHALEN *et al.* (1987).

*Symbols as in Figure 2.

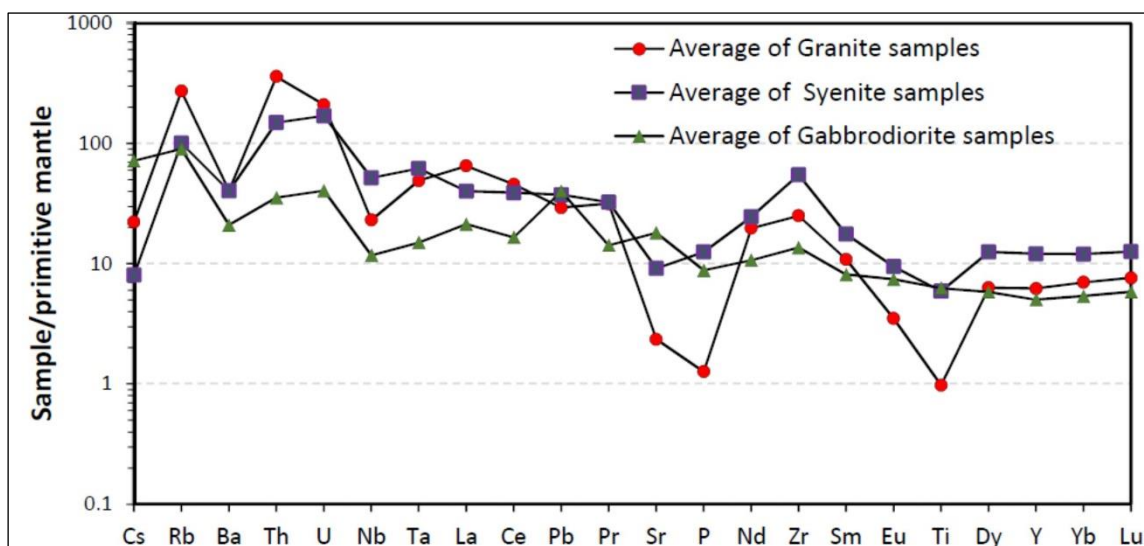


Figure 5. Primitive mantle-normalized element distributions for the intrusive rocks obtained from the BM intrusion.

Source: McDonough and Sun (1995).

Sample number	Fg112	Fg32	Fg18	Fg9	Fg99 Quartz monzonite	Fg2 Quartz monzonite	Fg75 Monzodiorite	Fg108 Monzodiorite	Fg79 Granite
Type rock	Granite	Granite	Granite	Granite					
Oxides (wt%)									
SiO ₂	75.21	73.11	77.94	74.02	60.44	63.84	51.67	54.87	72.73
TiO ₂	0.17	0.25	0.07	0.21	1.25	1.11	1.49	1.02	0.28
Al ₂ O ₃	13.29	14.08	11.48	13.62	16.51	15.57	18.11	17.86	14.03
Fe ₂ O ₃ *	0.59	1.57	0.37	1.39	1.32	1.79	3.03	2.97	1.55
MnO	0.01	0.04	0.01	0.04	0.06	0.08	0.17	0.16	0.03
MgO	0.16	0.24	0.07	0.19	2.87	1.28	7.06	7.21	0.27
CaO	0.17	0.22	0.12	0.31	7.67	5.23	10.03	9.62	0.21
Na ₂ O	3.68	3.48	3.21	4.12	8.18	5.46	3.21	3.50	3.52
K ₂ O	4.93	6.37	5.49	5.34	0.89	4.63	1.73	1.36	6.42
P ₂ O ₅	0.01	0.04	0.01	0.03	0.26	0.25	0.29	0.08	0.04
Total	98.22	99.40	98.77	99.27	99.46	99.25	96.78	98.64	99.1
Trace elements (ppm)									
Ba	271.00	307.00	236.11	217.00	98.24	433.00	159.61	116.97	305.97
Ce	40.13	109.85	41.72	82.10	69.97	60.012	31.293	24.11	109.48
Co	1.00	nd	1.00	nd	nd	nd	40.58	36.43	nd

Sample number Type rock	Fg112 Granite	Fg32 Granite	Fg18 Granite	Fg9 Granite	Fg99 Quartz monzonite	Fg2 Quartz monzonite	Fg75 Monzo diorite	Fg108 Monzo diorite	Fg79 Granite
Cr	10.00	8.95	30.00	10.11	30.01	10.00	220.26	209.76	8.88
Cs	0.34	0.48	0.32	0.72	0.12	0.22	1.21	1.80	0.48
Dy	3.49	5.50	1.80	4.97	7.00	9.85	3.63	4.18	5.45
Er	2.86	3.41	1.31	3.23	3.88	6.38	2.36	2.80	3.40
Eu	0.32	0.71	0.65	0.30	1.76	1.14	1.20	1.08	0.71
Ga	16.89	22.39	20.00	19.10	20.00	25.94	17.91	16.86	22.37
Gd	2.97	5.28	2.08	4.56	6.68	8.247	3.51	3.64	5.31
Hf	6.59	8.33	9.87	8.31	7.20	17.89	3.86	3.01	8.29
Ho	0.76	1.18	0.40	1.01	1.36	2.20	1.00	0.86	1.15
La	21.01	60.52	22.77	45.98	26.66	25.38	16.52	11.09	60.58
Lu	0.46	0.60	0.29	0.59	0.62	1.09	0.40	0.39	0.64
Nb	13.50	19.47	7.41	16.01	19.28	49.00	10.45	5	19.45
Nd	12.33	35.30	14.01	26.10	30.10	30.24	13.28	13.45	35.30
Ni	6.01	nd	4.10	0.80	12.38	1.29	83.64	56.98	nd
Pb	5.01	2.77	4.10	6.35	8.20	2.98	4.98	7.01	2.78
Pr	3.83	11.63	4.28	8.57	8.75	7.76	4.07	3.15	11.67
Rb	118.00	199.89	123.10	180.00	23.19	97.45	56.08	52.18	197.62
Sm	2.61	6.16	2.15	4.90	6.71	7.60	3.16	3.42	6.20
Sn	5.00	4.00	1.00	5.99	6.10	3.14	5.99	2.03	3.86
Sr	40.94	63.00	29.10	36.12	163.00	199.35	391.99	325.93	63.01
Ta	1.50	1.89	2.01	1.79	1.29	3.30	0.68	0.43	1.88
Tb	0.53	0.86	0.31	0.79	1.11	1.50	0.53	0.65	0.86
Th	30.30	27.00	30.00	30.00	9.46	14.50	1.70	3.97	27.19
Tm	0.45	0.56	0.24	0.56	0.62	1.01	0.29	0.36	0.57
U	4.54	3.85	4.60	4.31	3.13	3.65	0.64	0.98	3.76
V	5.01	7.00	5.01	6.99	140.00	66.47	235.14	186.48	6.85
W	2.03	3.20	1.00	2.00	2.32	1.00	1.34	1.15	3.01
Y	23.50	34.02	11.20	30.79	40.47	63.57	19.42	23.74	33.92
Yb	3.00	3.55	1.46	3.66	3.97	6.63	2.02	2.71	3.74
Zn	9.00	nd	10.00	nd	nd	nd	99.41	77.14	nd
Zr	211.04	312.26	189.69	289.35	339.89	809.75	165.21	120.91	309.79

Note: nd= not detected

*Total Fe as Fe₂O₃

Table 1. Major and trace element chemical compositions of the samples selected from the BM intrusion
Source: Authors (2020).

Sample number Rock type Position	Diorite Gh015 Core	Diorite Gh015 Rim	Diorite Gh068 Core	Diorite Gh068 Rim	Gh084 Syenite Core	Gh084 Syenite Rim	Gh078 Syenite Rim	Gh078 Syenite Core
<i>SiO₂</i>	48.11	49.58	48.68	47.39	50.06	48.01	49.87	47.91
<i>TiO₂</i>	0.64	0.46	0.76	0.65	0.38	0.75	0.62	1.19
<i>Al₂O₃</i>	7.04	5.66	6.65	7.32	5.32	6.53	5.34	8.84
<i>FeO</i>	18.20	17.69	18.11	18.43	18.34	19.11	17.12	16.10
<i>MnO</i>	0.51	0.40	0.44	0.46	0.47	0.52	0.87	0.75
<i>MgO</i>	11.29	12.23	11.38	11.03	11.84	10.83	12.98	11.55
<i>CaO</i>	11.88	11.79	11.99	11.99	11.89	11.61	11.45	11.25
<i>Na₂O</i>	1.13	0.98	1.14	1.16	0.98	1.20	0.91	1.17
<i>K₂O</i>	0.66	0.51	0.64	0.68	0.47	0.64	0.45	0.59
<i>Cr₂O₃</i>	0.00	0.00	0.04	0.00	0.01	0.00	0.00	0.00
<i>Total</i>	99.45	99.30	99.83	99.12	99.76	99.19	99.61	99.37
<i>Number of cations on the basis of 23 oxygen</i>								
<i>Si</i>	7.00	7.16	7.06	6.94	7.23	7.03	7.12	6.88
<i>Al^{IV}</i>	1.00	0.84	0.94	1.06	0.77	0.97	0.88	1.12
<i>Al^{VI}</i>	0.21	0.13	0.20	0.21	0.14	0.15	0.02	0.37
<i>Al^{total}</i>	1.21	0.96	1.14	1.26	0.91	1.13	0.90	1.50
<i>Ti</i>	0.07	0.05	0.08	0.07	0.04	0.08	0.07	0.13
<i>Cr</i>	0.00	0.00	0.00	0.00	0.00	0.00	0.00	0.00
<i>Fe⁺³</i>	0.51	0.59	0.40	0.49	0.51	0.56	0.89	0.59
<i>Fe⁺²</i>	1.70	1.55	1.80	1.77	1.70	1.78	1.16	1.34
<i>Mn</i>	0.06	0.05	0.05	0.06	0.06	0.06	0.11	0.09
<i>Mg</i>	2.45	2.64	2.46	2.41	2.55	2.36	2.76	2.47
<i>Ca</i>	1.85	1.82	1.86	1.88	1.84	1.82	1.75	1.73
<i>Na</i>	0.32	0.28	0.32	0.33	0.27	0.34	0.25	0.33
<i>K</i>	0.12	0.09	0.12	0.13	0.09	0.12	0.08	0.11
<i>OH[*]</i>	2.00	2.00	2.00	2.00	2.00	2.00	2.00	2.00
<i>Total</i>	18.50	18.16	18.44	18.60	18.11	18.41	17.98	18.66
<i>(Ca+Na)_(B)</i>	2.00	2.00	2.00	2.00	2.00	2.00	2.00	2.00
<i>Na_(B)</i>	0.15	0.18	0.14	0.12	0.16	0.18	0.25	0.27
<i>(Na+K)_(A)</i>	0.29	0.19	0.30	0.34	0.20	0.28	0.09	0.17
<i>Mg/(Mg+Fe⁺²)</i>	0.59	0.63	0.58	0.58	0.60	0.57	0.70	0.65
<i>Fe⁺²/(Mg+Fe⁺²)</i>	0.41	0.37	0.42	0.42	0.40	0.43	0.30	0.35
<i>Fe⁺³/(Fe⁺³+Al^{VI})</i>	0.71	0.82	0.67	0.70	0.79	0.78	0.98	0.61
<i>Al^{IV}/(Al^{IV}+Al^{VI})</i>	0.17	0.13	0.18	0.16	0.15	0.14	0.02	0.25

Table 2. Representative electron microprobe analysis of amphiboles from the BM intrusion.

Source: Authors (2020).

DISCUSSION

CRYSTALLIZATION CONDITIONS

THERMOBAROMETRY

The evolution of intrusion body requires information about the emplacement depth of intrusion. Hornblende chemistry is as a useful tool for determining of magmatic crystallization pressure of calc-alkaline igneous rocks (e.g., ANDERSON, SMITH, 1995; STEIN, DIETL, 2001; ERNST, 2002). Although the computed pressure may reflect the level at which the hornblende crystallizes rather than the pressure at which the granitoid rock consolidates (AGUE, 1997). Therefore, Al-hornblende barometry must be used in quartz+ plagioclase+ alkali feldspar+ biotite+ hornblende+ titanite+ magnetite/ilmenite mineral assemblage in granitoid rocks (HELMY *et al.*, 2004; LEAKE, SAID, 1994; AGUE, 1997). The mineral assemblage limited compositional influences and so calculated pressure is as crystalized pressure of magma (ANDERSON, SMITH, 1995). In the BM intrusion, all selected samples have the above mineral assemblage, which is an important prerequisite for Al- hornblende barometry. In addition, some limitation such as Si<7.3 apfu, Ca ≥1.6 apfu, Fe# <0.65, Al# <0.21 and Mg/(Mg+Fe+2) >0.5 should be used for Al-barometric applications (HAMMARSTROM, ZEN, 1986; ANDERSON, SMITH, 1995; RIDOLFI *et al.*, 2010). Thus, the selected magnesiohornblende satisfy the criteria established.

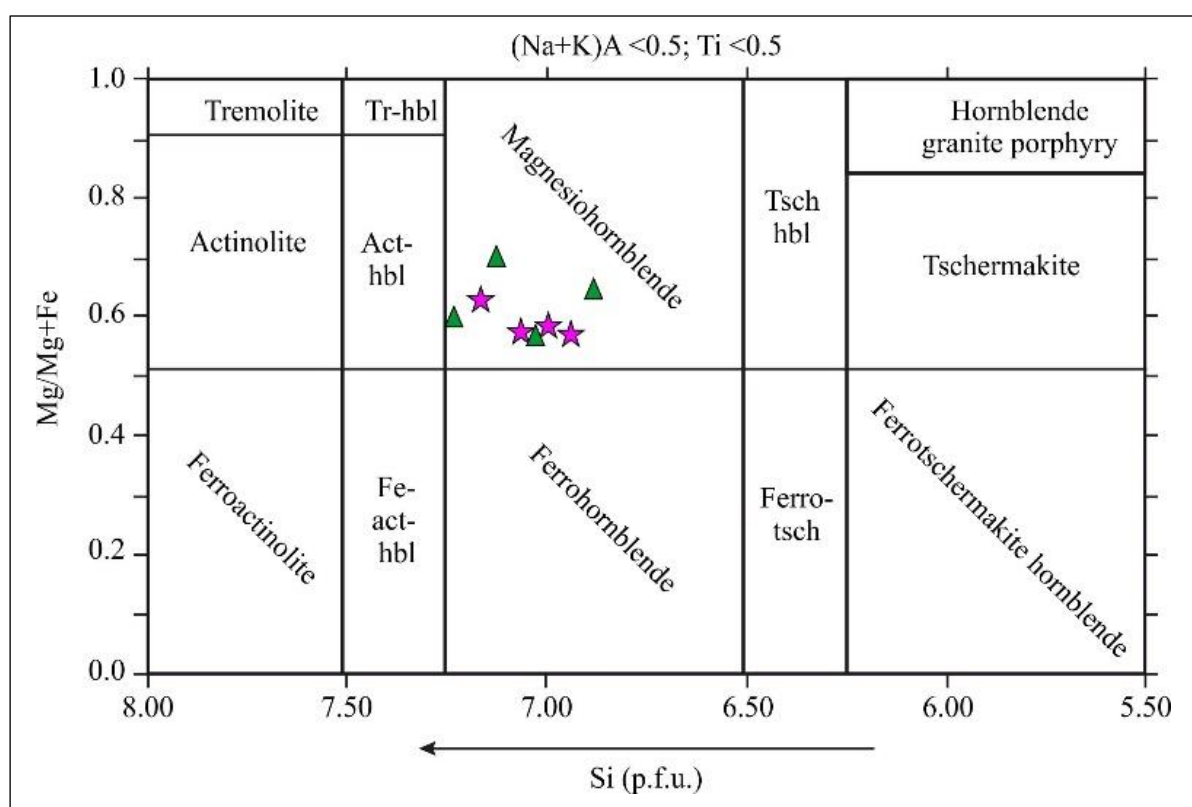


Figure 6. Plot of Mg/(Mg+Fe) against Si of amphibole classification.

Source: LEAK (1997).

*Symbols as in Figure 2.

Researchers present the various geobarometry with Al-content in hornbelend (HAMMARSTROM, ZEN 1986; HOLLISTER *et al.* 1987; SCHMIDT 1992; LEAKE, SAID 1994; AGUE and BRANDON 1996; ANDERSON 1996; STEIN and DIETL 2001; ERNST 2002; MOAZZEN and DROOP 2005; ZHANG *et al.* 2006; UCHIDA *et al.* 2007; ANDERSON *et al.* 2008; HOSSAIN *et al.* 2009). In the BM intrusion, pressure estimation with Schmidt (1992) and Blundy-Holland (1992) calibrations are adjusted with field observations and paragenetic associations. Thus, these calibrations are used for geobarometry of the BM intrusion and the emplacement pressure average of the BM intrusion for granite and diorite rocks are 2.14 and 2.33+0.6 kbar, respectively (Table 3). Anderson and Smith (1995) showed the Al-content of hornblende depends on pressure and temperature. Therefore, Anderson and Smith calibration (1995) was chosen to calculate the crystallization pressures of the studied

intrusion. The calculated pressure is about 2.70-3.71+0.6 kbar. According to considering errors (+0.6), the estimated pressures by using the methods of Schmidt (1992) and Blundy-Holland (1992) are lower than that of Anderson and Smith (1995) (Table 3).

ESTIMATION OF OXYGEN FUGACITY (FO₂) AND WATER CONTENT

Oxygen fugacity of magma is an effective factor in controlling magmatic processes (KILINC *et al.*, 1983; MORETTI, 2005; BOTCHARNIKOV *et al.*, 2005). Oxygen fugacity has a significant effect on the temperature of liquidus, crystal-melt component, sequence of crystallization and type of crystalized minerals. Therefore, oxygen fugacity is one of the important factors in determining the physicochemical conditions governing on the crystallization of an intrusive mass. Coexistence and chemical compositions of minerals show approximately the amount of oxygen fugacity. For example, Mg-rich amphibole, euhedral titanite and or magnetite are as a primary crystalized phase in magma which refer to partly oxidized magma (KUMAR, RINO, 2006; RIDOLFI *et al.*, 2010; ENAMI *et al.*, 1993). Fe/(Fe+Mg) ratios of amphiboles from the BM intrusion vary from 0.30 to 0.43 (Table 2) which are relatively low. In the Fe/(Fe+Mg) vs. AlIV diagram (Figure 7a) the positions of amphiboles reveal crystallization under intermediate fO₂ conditions.

AlVI content of amphiboles is also very sensitive to the water content of magmas (RIDOLFI *et al.*, 2010). Using the formulation of Ridolfi *et al.* (2010), the water content of melt for the center of amphiboles is 5.69 to 6.05 wt.% and for the rim of amphiboles is 5.07 to 5.80 wt.% (Table 4 and Fig 7b). the water content of the BM intrusion is adjusted to subduction zone (HAMZEII, 2013).

Sample number Rock type Position	Equations	Gh15 Diorite Core	Gh15 Diorite Rim	Gh68 Diorite Core	Gh68 Diorite Rim	Gh84 Syenite Core	Gh84 Syenite Rim	Gh78 Syenite Rim	Gh78 Syenite Core
HAMMARSTRO M and ZEN (1986)	$P ((\pm 3.0 \text{ kbar}) = -3.92 + 5.03 A^{\text{total}})$	2.15	0.93	1.80	2.44	0.64	1.75	0.60	3.61
HOLLISTER <i>et al.</i> (1987)	$P (\pm 1.0 \text{ kbar}) = -4.67 + 5.64 A^{\text{total}}$	2.05	0.68	1.66	2.37	0.35	1.59	0.31	3.68
JOHNSON and RUTHERFORD (1989)	$P (\pm 0.5 \text{ kbar}) = -3.46 + 4.23 A^{\text{total}}$	1.64	0.62	1.35	1.89	0.37	1.31	0.34	2.87
SCHMIDT (1992)	$P (\pm 0.6 \text{ kbar}) = -3.01 + 4.76 A^{\text{total}}$	2.73	1.58	2.41	3.01	1.30	2.35	1.27	4.11
BLUNDY and HOLLAND (1992)	$P (\text{kbar}) = -3.53 + 5.03 A^{\text{total}}$	2.54	1.32	2.19	2.83	1.03	2.14	0.99	4.00
ANDERSON and SMITH (1995)	$P (\pm 0.6 \text{ kbar}) = 4.76 A^{\text{total}} - 3.01 - \{[T_A - 675]/85\} * \{0.53 A^{\text{total}} + 0.005294[T_A - 675]\}$	2.85	2.70	3.00	2.89	3.71	2.83	3.44	2.70
P_{average}		2.64	1.45	2.30	2.92	1.17	2.25	1.13	4.05
Temperature (°C), VYHNAL <i>et al.</i> (1991)	$T (\text{°C}) = 25.3 P_{\text{ave.}}(\text{kbar}) + 654.9$	721.61	691.63	713.08	728.72	684.39	711.70	683.47	757.46
Oxygen fugacity (Log f_{O_2}) WONES (1989)	$\text{Log } f_{\text{O}_2} = -30930/T_A + 14.98 + 0.142 (P_{\text{average}} - 1)/T_1$	-16.11	-17.08	-16.38	-15.89	-17.32	-16.43	-17.35	-15.03

Table 3. Estimated pressure, temperature and oxygen fugacity of crystallization for intrusive rocks of the BM area using different proposed equations

T_A = temperature calculated from the mineral pairs by using Vyhnal *et al.* (1991) equation.

Source: HAMMARSTROM and ZEN (1986); HOLLISTER *et al.* (1987); SCHMIDT (1992); BLUNDY and HOLLAND (1992); ANDERSON and SMITH (1995); VYHNAL *et al.* (1991); WONES (1989).

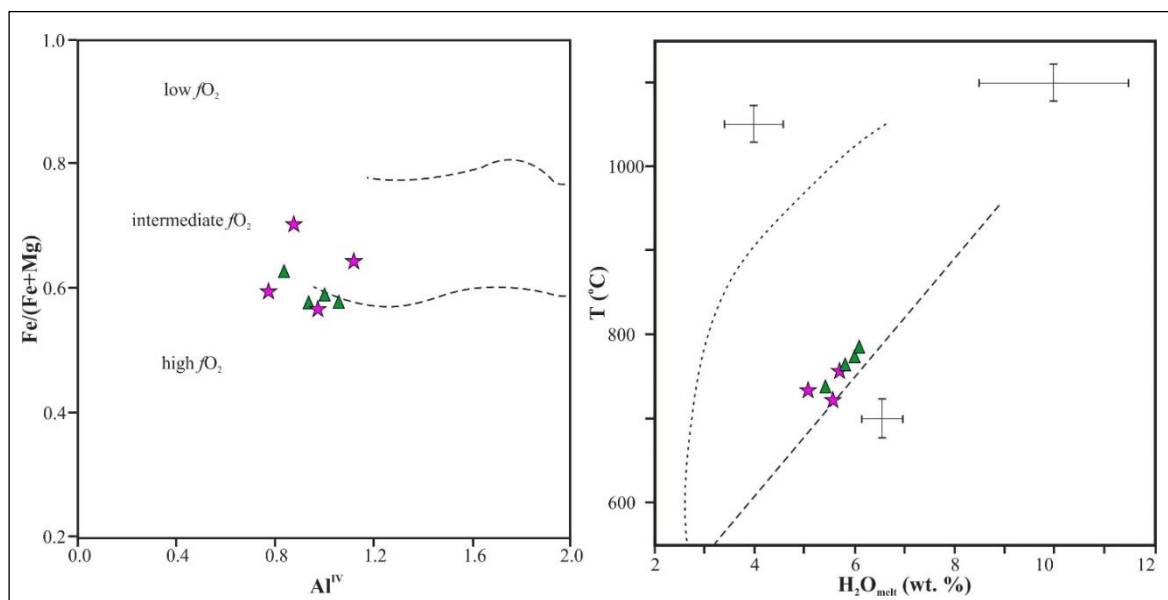


Figure 7. Fe/(Fe+Mg) vs. AlIV diagram for amphiboles (ANDERSON and SMITH, 1995), b) T-H₂O melt diagram for amphiboles (RIDOLFI *et al.*, 2010) (maximum errors on P, T and log fO₂ are given in Table 4).

* Symbols as in Figure 2.

Source: ANDERSON and SMITH (1995); RIDOLFI *et al.* (2010).

Rock type Sample number Position	Diorite Gh015 Core	Diorite Gh015 Rim	Diorite Gh068 Core	Diorite Gh068 Rim	Syenite Gh084 Core	Syenite Gh084 Rim	Syenite Gh078 Rim
Temperature (°C)	772.82	737.14	784.73	763.95	758.48	724.07	734.12
uncertainty (σest)	22.00	22.00	22.00	22.00	22.00	22.00	22.00
Pressure (MPa)	108.92	76.89	118.29	98.64	97.08	70.70	69.95
uncertainty (Max error)	11.98	8.46	13.01	10.85	10.68	7.78	7.69
continental depth (km)	4.11	2.90	4.47	3.73	3.67	2.67	2.64
ΔNNO	0.71	1.12	0.61	0.67	0.61	1.01	1.41
Oxygen fugacity (log fO ₂) (bars)	-13.74	-14.16	-13.57	-13.98	-14.17	-14.60	-13.96
uncertainty (σest)	0.40	0.40	0.40	0.40	0.40	0.40	0.40
H ₂ O melt (wt.%)	5.98	5.42	6.05	5.80	5.69	5.56	5.07
uncertainty	0.40	0.40	0.40	0.40	0.40	0.40	0.40

Table 4. Hornblende geothermobarometric results from the BM intrusion

Source: RIDOLFI *et al.* (2010).

CONCLUSION

The BM intrusion is composed of various plutonic rocks including granite, syenite, monzodiorite, diorite, and gabbrodiorite. Samples are metaluminous to slightly peraluminous. Mafic minerals in the plutonic rocks are biotite and hornblende. Mineral chemistry and whole rock analyses of the BM intrusion show a calc-alkaline to alkaline affinity. Amphibole compositions of the BM intrusion are calcic and magnesiohornblende. Results of thermobarometric calculations on the BM intrusion samples indicate multi-stage crystallization in the upper crust. The dioritic part was formed under relatively high pressure (ave. 2.33+0.6 kbar) and high temperature (ave. 713 oC). The granitic part was formed under slightly low pressure (ave. 2.14+0.6 kbar) and low temperature (ave. 693 oC) than the dioritic part. The melt is represented by intermediate log fO₂ values (-13.74- -14.60) and high H₂O content (5.07-6.05 wt.%).

REFERENCES

- AGEMAR, T.; WORNER, G.; HEUMANN, A. Stable isotopes and amphibole chemistry on hydrothermally altered granitoids in the North Chilean Precordillera: a limited role for meteoric water?. **Contribution to Mineralogy and Petrology**, n.136, 1997. p. 331-344.,
- AGUE, J. J. Thermodynamic calculation of emplacement pressures for batholithic rocks, California: Implications for the aluminum-in-hornblende barometer. **Geology**, 25, 1997. p. 563-566.
- AGUE, J. J.; BRANDON, M. T.; Regional tilt of the Mount Stuart batholiths, Washington, determined using aluminum in hornblende barometry: Implications for northward translation of Baja British Columbia. **Geological Society of America Bulletin**, 108, 1996. p. 471-88.
- ANDERSON, J. L.; BARTH, A. P.; WOODEN, J. L.; MAZDAB, F. Thermometers and thermobarometers in granitic systems. **Reviews in Mineralogy and Geochemistry**, 69, 2008. p. 121-42.,
- ANDERSON, J. L. Status of thermobarometry in granitic batholiths. **Earth sciences**, 87, 1996. p. 125-138.
- ANDERSON, J. L.; SMITH, D. R. The effects of temperature and fO₂ on the Al-inhornblende barometer. **American Mineralogist**, 80, 1995. p. 549-559.
- AZIZI, H.; ASAHIARA, Y. Juvenile granite in the Sanandaj-Sirjan zone, NW Iran: Late Jurassic-Early Cretaceous arc-continent collision. **International Geology Review**, n.55, 2013, p. 1523-1540.,

AZIZI, H.; ASAHLARA, Y.; MEHRABI, B.; CHUNG, S. L. Geochronological and geochemical constraints on the petrogenesis of high-K granite from the Suffiabad area, Sanandaj-Sirjan Zone, NW Iran.

Chemie der Erde- Geochem, 71, 2011b. p. 363-376.,

AZIZI, H.; BEIRANVAND, M. Z.; ASAHLARA, Y. Zircon U-Pb ages and petrogenesis of a tonalite-trondhjemite-granodiorite (TTG) complex in the Northern Sanandaj-Sirjan Zone, Northwest Iran: evidence for Late Jurassic arc-continent collision. **Lithos**, 216-217, 2015a. p. 178-195.,

AZIZI, H.; CHUNG, S. L.; TANAKA, T.; ASAHLARA, Y. Isotopic dating of the Khoy metamorphic complex (KMC), northwestern Iran: a significant revision of the formation age and magma source.

Precambrian Research, n. 185, 2011a. p. 87-94.,

AZIZI, H.; MOHAMMADI, K.; ASAHLARA, Y.; TSUBOI, M.; DANESHVAR, N.; MEHRABI, B. Strongly peraluminous leucogranite (Ebrahim-Attar granite) as evidence for extensional tectonic regime in the Cretaceous, Sanandaj-Sirjan zone, northwest Iran. **Chemie der Erde- Geochem.**, 76, 2016. p. 529-541.

AZIZI, H.; NAJARI, M.; ASAHLARA, Y.; CATLOS, E. J.; SHIMIZU, M.; YAMAMOTO, K. U-Pb zircon ages and geochemistry of Kangareh and Taghiabad mafic bodies in northern Sanandaj-Sirjan Zone, Iran: Evidence for intra-oceanic arc and back-arc tectonic regime in Late Jurassic. **Tectonophysics**, n.660, 2015b, p. 47-64.,

BLUNDY, J. D.; HOLLAND, T. J. B. Calcic amphibole equilibria and a new amphibole-plagioclase geothermometer: Reply to the comments of Hammarstrom and Zen, and Rutherford and Johnson. **Contributions to Mineralogy and Petrology**, n. 111, 1992. p. 269-272.

BOTCHARNIKOV, R. E.; KOEPKE, J.; HOLTZ, F.; MCCAMMON, C.; WILKE, M.; The effect of water activity on the oxidation and structural state of Fe in a ferro-basaltic melt. **Geochimica et Cosmochimica Acta**, 69 (21), 2005. p. 5071-5085.

CHAPPELL, B. W.; WHITE, A. J. R. Two contrasting granite types. **Pacific Geology**, 8, 1974. p. 173-174.

ENAMI, M.; SUZUKI, K.; LIOU, J. G.; BIRD, D. K. Al-Fe³⁺ and F-OH substitutions in titanite and constrains on their P-T dependence. **European Journal of Mineralogy**, 5(2), 1993. p. 231-291.

ERNST, W. G. Paragenesis and thermobarometry of Ca-amphiboles in the Barcroft granodioritic pluton, central White Mountains, eastern California. **American Mineralogist**. 87, 2002. p. 478-90.

FROST, B. R.; FROST, C. D. A geochemical classification for feldspathic igneous rocks. **Journal of Petrology**, 49, 2008. p. 1955-1969.,

HAMMARSTROM, J. M.; ZEN, E. A. Aluminum in hornblende: an empirical igneous geobarometer. **American Mineralogist**, 71, 1986. p. 1297-1313.

HAMZEII, Z. **Petrogenesis of the Nasrand intrusive mass, SE Ardestan..** Thesis (M.Sc in geology) University of Tehran, Tehran, Iran, 2013. 115 pp. (in Persian with English Abstract).

HASSANZADEH, J.; STOCKLI, D. F.; HORTON, B. K.; AXEN, G. J.; STOCKLI, L. D.; GROVE, M.; SCHMITT, A.K.; WALKER, J. D. U-Pb zircon geochronology of late Neoproterozoic. Early Cambrian granitoids in Iran: implications for paleogeography, magmatism, and exhumation history of Iranian basement. **Tectonophysics**, 451, 2008. p. 71-96.

HELMY, H. M.; AHMED, A. F.; EL MAHALLAWI, M. M.; ALI, S. M. Pressure, temperature and oxygen fugacity conditions of calc-alkaline granitoids, Eastern Desert of Egypt, and tectonic implication. **Journal of African Earth Science**, 38, 2004. p. 255-268.

HOLLISTER, L. S.; GRISSOM, G. E.; PETERS, E. K.; STOWELL, H. H.; SISSON, V. R. Confirmation of the empirical correlation of Al in hornblende with pressure of solidification of calc-alkaline plutons. **American Mineralogist**, n. 72, 1987. p. 231-239.,

HOSSAIN, I.; TSUNOGAE, T.; RAJESH, H. M. Geothermobarometry and fluid inclusions of dioritic rocks in Bangladesh: Implications for emplacement depth and exhumation rate. **Journal of Asian Earth Sciences**, 34, 2009. 731-739.

JOHNSON, M. C.; RUTHERFORD, M. J. Experimental calibration of an aluminum-in-hornblende geobarometer applicable to calc-alkaline rocks. **Geology**, 17(9), 1989. 837-841.

KILINC, A.; CARMICHAEL, I. S. E.; RIVERS, M. L.; SACK, R. O. The ferric-ferrous ratio of natural silicate liquids equilibrated in air. **Contributions to Mineralogy and Petrology**, 83, 1983. p. 136-140.

KUMAR, S.; RINO, V. Mineralogy and geochemistry of microgranular enclaves in Palaeoproterozoic Malanjkhand Granitoids, CENTRAL India: evidence of magma mixing, mingling and chemical equilibration. **Contributions to Mineralogy and Petrology**, 152 (5), 2006. p. 591-609.

LEAKE, B. E.; SAID, Y. A. Hornblende barometry of the Galway batholith, Ireland: An empirical test. **Mineralogy and Petrology**, 51, 1994. p. 243-250.

LEAKE, B. E. On aluminous and edenitic hornblendes. **Mineralogical Magazine**, 38, 1971. p. 389-407.

LEAKE, B. E.; WOOLLEY, A. R.; ARPS, C. E. S.; BIRCH, W. D.; GILBERT, M. C.; GRICE, J. D.; HAWTHORNE, F. C.; KATO, A.; KISCH, H. J.; KRIVOVICHEV, V. G.; LINTHOUT, K.; LAIRD, J.; MANDARINO, J. A.; MARESCH, W. V.; NICKEL, E. H.; ROCK, N. M. S.; SCHUMACHER, J. C.; SMITH, D. C.; STEPHENSON, N. C. N.; UNGARETTI, L.; WHITTAKER, E. J. W.; YOUZHI, G. Nomenclature of amphiboles: Report of the Subcommittee on Amphiboles of the International Mineralogical Association, Commission on New Minerals and Mineral Names. **American Mineralogist**, 82, 1997. p. 1019-1037.

LEAKE, B. E.; WOOLLEY, A. R.; BIRCH, W. D.; BURKE, E. A. J.; FERRARIS, G.; GRICE, J. D.; HAWTHORNE, F. C.; KISCH, H. J.; KRIVOVICHEV, V. G.; SCHUMACHER, J. C.; STEPHENSON, N. C. N.; WHITTAKER, E. J. W. Nomenclature of amphiboles: Additions and revisions to the International Mineralogical Association's amphibole nomenclature. **American Mineralogist**, n. 89, 2004. p. 883-887.

MAHMOUDI, S.; CORFU, F.; MASOUDI, F.; MEHRABI, B.; MOHAJJEL, M. U-Pb dating and emplacement history of granitoid plutons in the northern Sanandaj-Sirjan Zone, Iran. **Journal of Asian Earth Sciences**, n. 41, 2011. p. 238-249.

MANIAR, P. D.; PICCOLI, P. M. Tectonic discrimination of granitoids. **Geological Society of America Bulletin**, n. 101, 1989. p. 635-643.

MIDDLEMOST, E. A. K. Magmas and Magmatic Rocks, An Introduction to Igneous Petrology. Longman Group UK: London, 1985.

MOAZZEN, M.; DROOP, G. T. R. Application of mineral thermometers and barometers to granitoid igneous rocks: the Etive Complex, W Scotland. **Mineralogy and Petrology**, n. 83, p. 27-53, 2005.

MOHAJJEL, M.; FERGUSSON, C. Jurassic to Cenozoic tectonics of the Zagros Orogen in northwestern Iran. **International Geology Review**, n. 56, 2014. p. 263-287.

MOHAJJEL, M.; FERGUSSON, C. L.; SAHANDI, M. R. Cretaceous-Tertiary continental collision, Sanandaj-Sirjan Zone, western Iran. **Journal of Asian Earth Sciences**, 21, 2003. p. 397-412.

MOODY, J. B.; MEYER, D.; JENKINS J. E. Experimental characterization of the greenschist/amphibolite boundary in mafic systems. **American Journal of Science**, 283, 1983. p. 48-92.

MORETTI, R. Polymerization, basicity, oxidation state and their role in ionic modelling of silicate melts. **Geophysics**, n. 48, 2005. p. 583-608.

RIDOLFI, F.; RENZULLI, A.; PUERINI, M.; Stability and chemical equilibrium of amphibole in calc-alkaline magmas: an overview, new thermobarometric formulations and application to subduction-related volcanoes. **Contributions to Mineralogy and Petrology**, n. 160, 2010. p. 45-66.

RUTTER, M. J.; VAN DER LAAN, S. R.; WYLLIE, P. J. Experimental data for a proposed empirical igneous geobarometer: Aluminium in hornblende at 10 kbar pressure. **Geology**, 17, 1989. p. 897-900.

SCHMIDT, M. W. Amphibole composition in tonalite as a function of pressure: An experimental calibration of the Al-in-hornblende barometer. **Contributions to Mineralogy and Petrology**, 110, 1992. p. 304-310.

SHAHBAZI, H.; SIEBEL, W.; GHORBANI, M.; POURMOAFEE, M.; SEPAHI, A. A.; ABEDINI, M. V.; SHANG, C. K. The Almogholagh pluton, Sanandaj-Sirjan zone, Iran: geochemistry, U-(Th)-Pb titanite geochronology and implications for its tectonic evolution. **Neues Jahrbuch für Mineralogie – Abhandlungen**, 192, 2015. p. 85-99.

STEIN, E.; DIETL, C. Hornblende thermobarometry of granitoids from the Central Odenwald (Germany) and their implications for the geotectonic development of the Odenwald. **Mineralogy and Petrology**, 72. 2001. p. 185-207.

TILLMAN, J. E.; POOSTI, A.; ROSSELLO, S.; ECKERT, A. Structural evolution of Sanandaj-Sirjan Ranges near Esfahan, Iran. **American Association of Petroleum Geologists Bulletin**, 65, 1981. p. 674-687.

UCHIDA, E.; ENDO, S.; MAKINO, M. Relationship between solidification depth of granitic rocks and formation of hydrothermal ore deposits. **Resource Geology**, 57, 2007. p. 47-56.

VYHNAL, C. R.; MCSWEEN, H. Y.; SPEER, J. A. Hornblende chemistry in southern Appalachian granitoids: Implications for aluminum hornblende thermobarometry and magmatic epidote stability. **American Mineralogist**, 76, 1991. p. 167-88.

WHALEN, J. B.; CURRIE, K. L.; CHAPPELL, B. W. A-type granites: geochemical characteristics, discrimination and petrogenesis. **Contributions to Mineralogy and Petrology**, 95, 1987. p. 407-419.

YAJAM, S.; MONTERO, P.; SCARROW, J. H.; GHALAMGHASH, J.; RAZAVI, S. M. H.; BEA, F. The spatial and compositional evolution of the Late Jurassic Ghorveh-Dehgolan plutons of the Zagros Orogen, Iran: SHRIMP zircon U-Pb and Sr and Nd isotope evidence. **Geologica Acta**, 13, 2015. p. 25-43.

ZHANG, S. H.; ZHAO, Y.; SONG, B. Hornblende thermobarometry of the Carboniferous granitoids from the Inner Mongolia Paleo-uplift: Implications for the tectonic evolution of the northern margin of North China block. **Mineralogy and Petrology**, 87, 2006. p. 123-141.

WONES, D. R.; Significance of the assemblage titanite+magnetite+quartz in granitic rocks. **American Mineralogist**, 74, 1989. p. 744-749.